Identification and correlation of Oligocene ignimbrites in well bores, Alamosa Basin (northern San Luis Basin), Colorado, by single-crystal laser-fusion $^{40}Ar/^{39}Ar$ geochronology of well cuttings

Brian S. Brister and William C. McIntosh
New Mexico Bureau of Geology and Mineral Resources, New Mexico Institute of Mining and Technology, Socorro, NM 87801

Abstract

The Alamosa Basin is the northern sub-basin of the San Luis Basin, Rio Grande rift, south-central Colorado. Within the Alamosa Basin is a lithologically complex, andesitic-to-rhyolitic Oligocene volcanic sequence that includes welded ignimbrites (ash-flow tuffs), non-welded tuffs, volcaniclastic sediments, and lava flows. Within this sequence, regional Oligocene ignimbrites can be recognized in the subsurface by combining well-cutting petrology, geophysical-log correlation, and $^{40}Ar/^{39}Ar$ geochronology of single crystals from selected well cuttings.

Single crystals dated in this study were selected using criteria designed to minimize contamination problems inherent to well-cutting samples. Where possible, phenocrysts of sanidine or biotite were separated from cutting fragments displaying distinctive eutaxitic welded tuff textures. Loose, matrix-free sanidine crystals picked directly from cuttings were also dated. Laser-fusion analyses of samples with sufficiently large and numerous single crystals revealed one or more well defined populations of single-crystal ages (2σ precision typically $\leq \pm 0.4$ Ma for individual crystals, $\leq \pm 0.2$ Ma for populations). These $^{40}Ar/^{39}Ar$ data allow subsurface ignimbrites to be correlated with regional ignimbrite chronology. Identified ignimbrites include the 27.3 Ma Carpenter Ridge Tuff , the 27.8 Ma Fish Canyon Tuff, and a member of the 30–29 Ma lower Treasure Mountain Group, all erupted from calderas in the 35–23 Ma San Juan volcanic field, and the 32.9 Ma Gribbles Park Tuff, erupted from the Bonanza caldera of the 38–30 Ma Central Colorado volcanic field. Regional ignimbrites recognized in selected wells by $^{40}Ar/^{39}Ar$ data are readily correlated using well-log data to undated ignimbrites in other wells.

Subsurface correlations constrained by geochronology demonstrate that the Conejos Formation from the San Juan Mountains, with possible contributions from the Central Colorado volcanic field, is thickest in the Monte Vista graben of the western half of the Alamosa Basin and is thin to absent in the eastern half. The Gribbles Park Tuff from the Bonanza caldera is interlayered with the Conejos Formation in the western half of the Alamosa Basin and is also present in the eastern half. Post-Conejos ignimbrites appear to have blanketed the entire region, implying subdued aggradational paleotopography. Inter-ignimbrite volcaniclastic sediments are thickest near the western margin of the graben. These formations record an early phase of regional Oligocene extension that is documented in other basins of the Rio Grande rift. The Santa Fe Group, which contains sanidine derived from regional ignimbrites, lies unconformably above the 27.3 Ma Carpenter Ridge Tuff, a distinctive seismic marker horizon. In contrast to the underlying Oligocene volcanic sequence, the Santa Fe Group thickens eastward into the Baca sub-graben and records the main episode of rift valley formation.

Introduction

Cuttings and logs from wells drilled in search of petroleum, water, or geothermal resources are routinely used to identify and correlate regional sedimentary formations. Although such wells commonly penetrate lavas and pyroclastic volcanic rocks, these strata are often largely ignored. Although this in part reflects lack of interest in volcanic rocks as reservoirs, it is also due to the difficulty in performing petrologic and geochemical identification and classification techniques on finely ground well cuttings. Well cuttings are commonly contaminated with materials from higher in the borehole or by unrecognized xenolithic or xenocrystic material. These contaminants complicate accurate geochemical or geochronological analyses of bulk samples of well cuttings. Analysis and interpretation of well-cutting data is also frequently complicated by incomplete or inaccurate collection of cuttings at the drill site, by uncertainties regarding the exact depths that the cuttings represent, by averaging of stratigraphic intervals, by blurring of stratigraphic contacts, or by omission of stratigraphic units.

This study represents an attempt to overcome some of the difficulties inherent in using cuttings to interpret subsurface volcanic stratigraphy by combining single-crystal $^{40}Ar/^{39}Ar$ dating with standard petrologic and well-log interpretation. The study area, the Alamosa Basin of south-central Colorado, has been penetrated by a series of petroleum and geothermal exploration holes to depths of 1,851–3,155 m. Previous petrologic study of cuttings (Brister and Gries 1994) established that the wells penetrated a sequence of volcanic and volcaniclastic rocks. This volcanic sequence was interpreted to be a buried part of the adjacent San Juan volcanic field (Lipman 2000). Many studies have examined the stratigraphy and chronology of the San Juan volcanic field and the adjoining, older Central Colorado volcanic field (e.g., Lipman et al. 1970; Epis and Chapin 1974; Steven and Lipman 1976; Lanphere 1988; McIntosh and Chapin 2004 this volume). Key regional stratigraphic markers within these volcanic fields are voluminous ignimbrites (ash-flow tuffs) erupted from calderas (Table 1). Brister and Gries (1994) suggested that some of these ignimbrites exist within the Alamosa Basin and can be correlated using well logs and petrology. The primary goal of the present study was to test and refine these correlations using $^{40}Ar/^{39}Ar$ geochronology.

Geometry and stratigraphy of Alamosa Basin

The San Luis Basin of south-central Colorado is one of a number of axial basins of the Rio Grande rift (Fig. 1; Chapin 1971; Chapin and Cather 1994). The northern part of the San

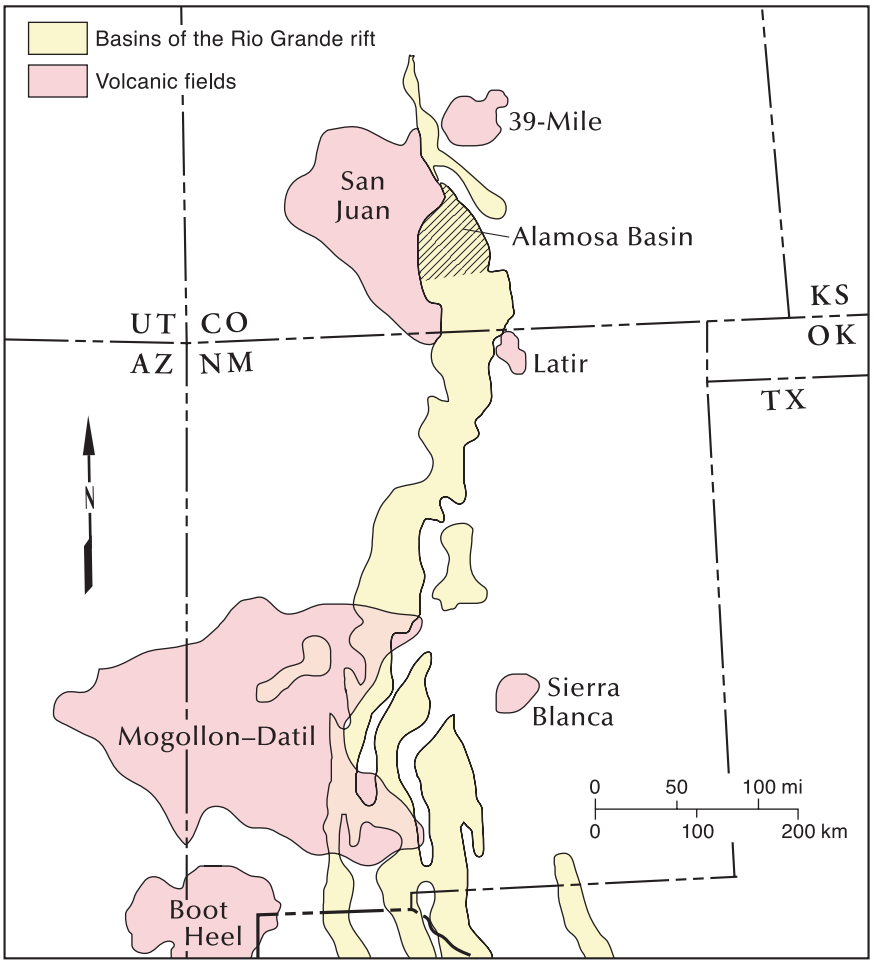

FIGURE 1—Index map of New Mexico and southern Colorado showing basins of the Rio Grande rift, major Oligocene volcanic fields, and the Alamosa Basin.

Luis Basin, known as the Alamosa Basin (Burroughs 1981), is bounded by the Sangre de Cristo Range to the east, the San Juan volcanic field to the west, and San Luis Hills to the south (Fig. 2). Well control and geophysical data define the general geometry of the Alamosa Basin (e.g., Cordell 1978; Burroughs 1981; Keller et al. 1984; Gries 1985; Brister and Gries 1994; Kluth and Shaftenaar 1994). The Alamosa Basin is one of the deepest basins of the rift in terms of thickness of rift-related fill (approximately 5.6 km [3.5 mi]; Brister and Gries 1994). The western part of the basin (Fig. 3) is the north-trending, east-tilted Monte Vista graben (Burroughs 1981) that resulted from reactivation of a pre-existing Laramide depression (Brister and Chapin 1994). The deeper, eastern part of the basin is the north-trending, east-tilted Baca graben (Burroughs 1981) that overlies a foundered Laramide highland (Brister and Gries 1994). The Monte Vista and Baca grabens are separated by the structurally elevated, north-trending Alamosa horst (Burroughs 1981).

The general stratigraphy of the Alamosa Basin has been established by examining the petrology of well cuttings (Brister and Gries 1994). In simplest terms, there are four main stratigraphic units present (Fig. 3). They are, from youngest to oldest: the late Oligocene to Pleistocene Santa Fe Group, an Oligocene volcanic and volcaniclastic sequence, a late Eocene (Laramide) red bed formation, and Precambrian crystalline basement. In the western half of the Alamosa Basin, all four units are interpreted to be present, whereas in the eastern half the Eocene is thin to absent. The base of the Oligocene volcanic sequence is an unconformable surface, the "late Eocene erosion surface" of Epis and Chapin (1975), developed upon pre-volcanic Eocene red beds in the western Monte Vista graben and Precambrian basement in the eastern Baca graben (Brister and Chapin 1994; Brister and Gries 1994).

TABLE 1—Ages and source calderas of selected regional ignimbrites from the San Juan and Central Colorado volcanic fields, Colorado. ** = mean of two or more published sample ages, * = ages increased by 1% to adjust for interlaboratory calibration related to differences in accepted monitor ages.

Ignimbrite	Caldera	$^{40}Ar/^{39}$ Ar age (Ma)	Mineral	References
San Juan volcanic field ignimbrites				
Sunshine Peak Tuff	Lake City	22.93 ± 0.02	sanidine	6
Nelson Mountain Tuff	San Luis	26.39 ± 0.08*	sanidine	3
Rat Creek Tuff	San Luis	26.71 ± 0.07*	biotite	3
Snowshoe Mountain Tuff	Creede	27.07 ± 0.10*	biotite	3
Carpenter Ridge Tuff	Bachelor	27.38 ± 0.12	sanidine	7
Fish Canyon Tuff	La Garita	27.84 ± 0.05	sanidine	2
Masonic Park Tuff	Mount Hope	28.60 ± 0.23*	biotite	5
Treasure Mountain Group				
Chiquito Peak Tuff	Platoro	28.41 ± 0.07**	sanidine	5
South Fork Tuff	Platoro/Summitville	28.76 ± 0.07	sanidine	5
Ra Jadero Tuff	Platoro/Summitville	28.77 ± 0.07**	sanidine	5
Ojito Creek Tuff	Platoro	29.1 ± 0.3	biotite	1
La Jara Canyon Tuff	Platoro	29.3 ± 0.3	biotite	1
Black Mountain Tuff	Platoro	29.4 ± 0.4	biotite	1
Conejos Formation lavas and tuffs		29.4 ± 33.1	biotite, hornblende	4,5
Central Colorado volcanic field ignimbrites				
Gribbles Park Tuff	Bonanza	32.90 ± 0.06	sanidine	7

References: **1**—Balsley 1994; **2**—Deino and Potts 1990; **3**—Lanphere 1988; **4**—Colucci et al. 1991; **5**—Lipman et al. 1996; **6**—Bove et al. 2000; **7**—McIntosh and Chapin 2004 this volume.

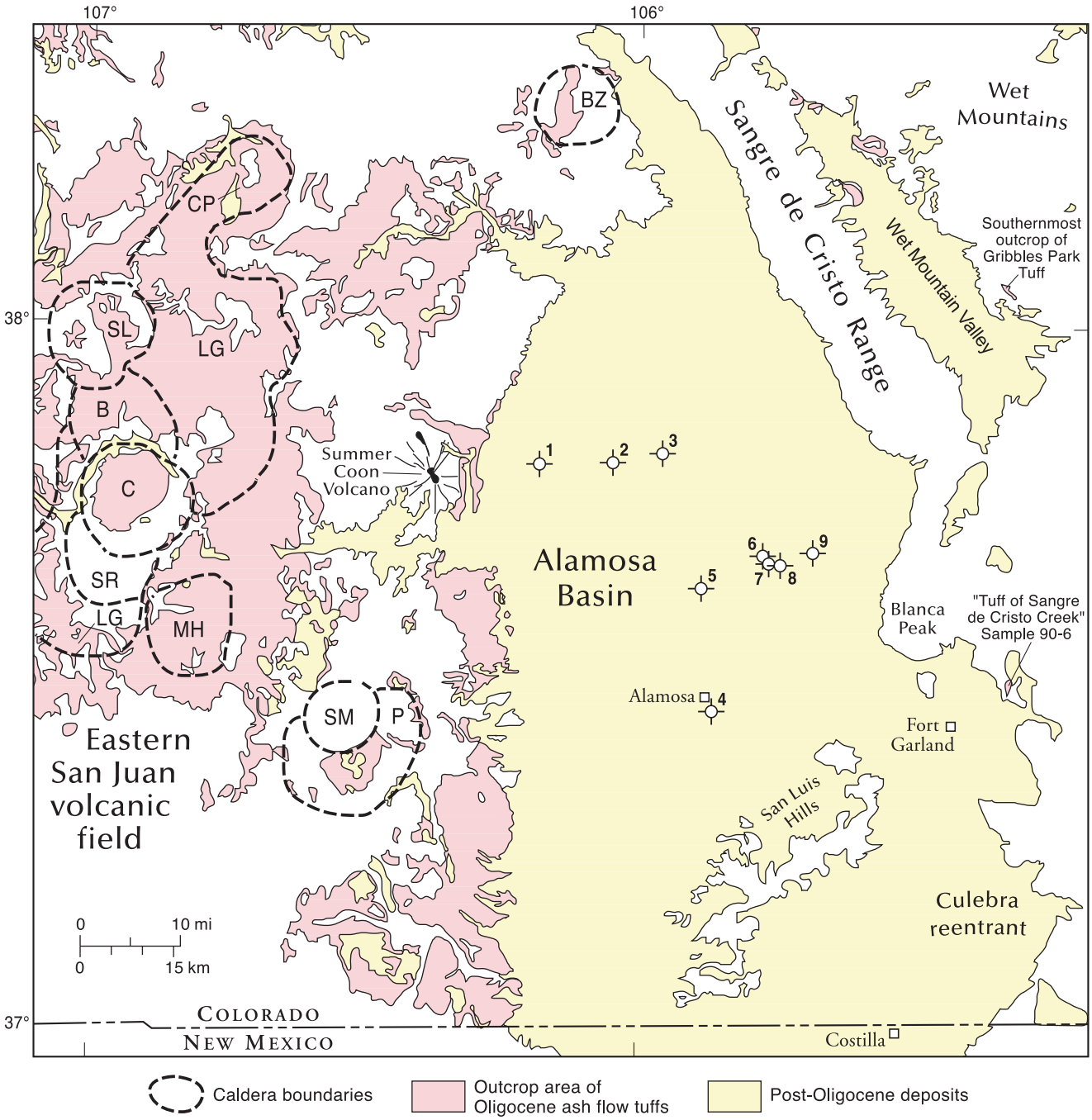

FIGURE 2—Simplified geologic map of south-central Colorado showing locations of Alamosa Basin wells studied (after Tweto 1979). Calderas depicted in the eastern part of the San Juan volcanic field are: **P** = Platoro, **SM** = Summitville, **LG** = La Garita, **MH** = Mount Hope, **B** = Bachelor, **C** = Creede, **SR** = South River, **SL** = San Luis, **CP** = Cochetopa Park (after Steven and Lipman 1976; Lipman et al. 1996; and Lipman 2000). The Bonanza caldera (**BZ**) is the southernmost caldera of the Central Colorado volcanic field.

Well data used in study

Wells in the Alamosa Basin and data availability

Minor gas produced from shallow water wells drew interest in the petroleum potential of the Alamosa Basin in the early 1950s (Gries 1985). At least 12 wells have been drilled in the basin for the purpose of exploration for petroleum or geothermal resources. Nine of those wells were selected for this study. These wells, numbered in this paper from west to east as wells 1 through 9 (Figs. 2, 4; Table 2) were drilled between 1951 and 1981. Well number 4 was drilled as a geothermal test (Phetteplace and Kunze 1983), whereas the others were petroleum exploration wells. None of these wells yielded evidence of economic petroleum resources. However, geothermal potential cannot be ruled out. Three additional petroleum exploration wells were drilled between 1989 and 1995 at basin margins (Brister and Chapin 1994; Watkins 1996), but are not considered in this paper.

Open-hole geophysical well logs for eight of the wells in Figure 4 are available from commercial sources. The types of well logs available vary by age of well. Spontaneous potential and electrical resistivity were found to be the most useful log types for correlation purposes in the volcanic

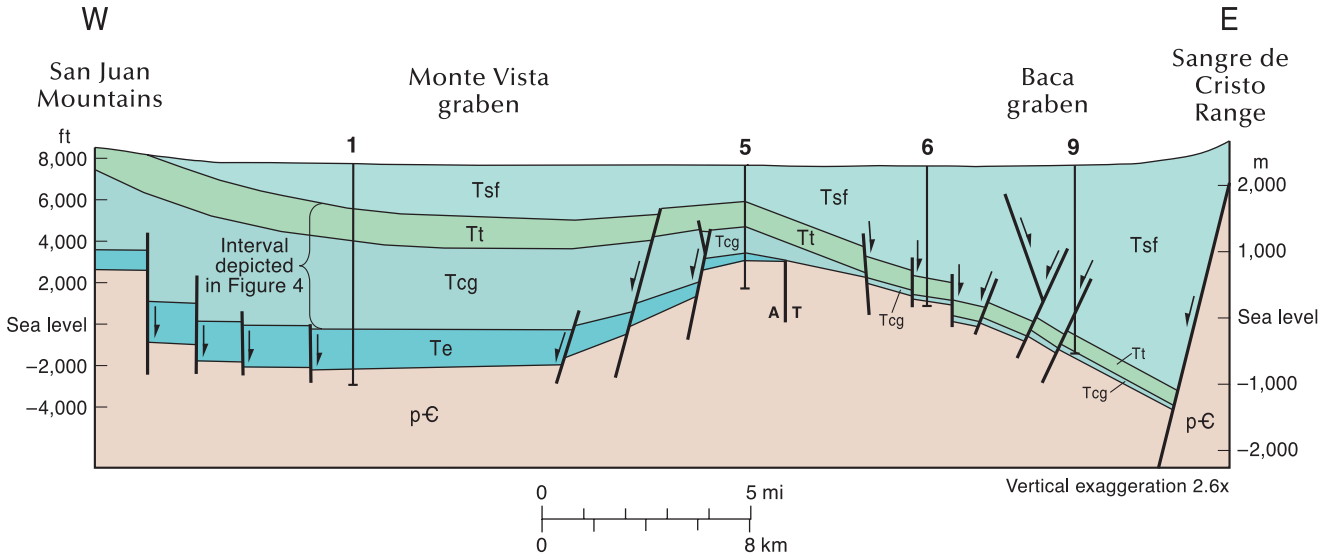

FIGURE 3—Generalized west-east structural cross section that depicts geometry and stratigraphic units within the Alamosa Basin as interpreted from seismic and well data. Figure simplified from Brister and Gries (1994). Abbreviations for stratigraphic units: **Tsf** = sedimentary units of the Santa Fe Group (upper Oligocene–Pleistocene), **Tt** = ignimbrites and interbedded volcaniclastic units derived from the San Juan volcanic field (Oligocene), **Tcg** = interbedded volcanic and volcaniclastic Conejos Formation and Gribbles Park Tuff (Oligocene), **Te** = Eocene red beds, **p€**= Precambrian crystalline basement. **A** = strike slip motion into the page, **T** = strike slip motion out of the page.

TABLE 2—Location and depth information for wells in the Alamosa Basin considered in this study. Formation depth data reported as top–base/thickness (ft).

Well #	1	2	3	4	5	6	7	8	9
Operator	Tennessee Gas	Orrin Tucker	W. F. Carr	Energy Services	Amerada Petroleum	Reserve Oil	W. F. Carr	Cougar Petroleum	Amoco-Mapco
Well name	State B #1	Thomas #1	Kennedy & Williams #1	Alamosa #1 Geothermal	Colorado State F #1	NBH Alamosa #1-33	J. M. Crow #1	Crow #1	Mapco State #1-32
Year drilled	1959	1951	1952	1981	1959	1979	1952	1981	1974
Location Sec. T R	14, 41N 7E	13, 41N 8E	11, 41N 9E	15, 37N 10E	16, 39N 10E	33, 40N 11E	4, 39N 11E	3, 39N 11E	32, 40N 12E
KB Elevation	7,675	7,606	7,574	7,550	7,569	7,539	7,536	7,537	7,600
Depth range/thickness (ft)									
Carpenter Ridge Tuff	2,072–2,152/80	3,650–3,800/150	4,114–4,178/64	2,530–2,590/60	1,744–1,792/48	5,154–5,172/18	5,630–5,686/56	6,105–6,208/103	8,620–8,690/70
Fish Canyon Tuff	2,368–2,536 168	3,884–4,010/126	4,212–4,350/138	2,590–2,740/150	1,792–1,940/148	5,172–5,268/96	5,686–5,804/118	6,270–6,428/158	8,700–9,000/300
Masonic Park Tuff (?)	Not recognized	Not recognized	4,759–4,902/143	2,920–3,160/240	2,190–2,320/130	5,536–5,686/150	6,082–6,240/158	6,578–6,744/166	9,060–9,188/118
Lower Treasure Mountain Group	3,434–3,488/54	5,212–5,268/56	5,414–5,520/ 06	3,580–3,700/120	2,430–2,490/60	5,916–6,012/96	6,294–6,392/98	6,802–6,928/126	9,252–9,324/72
Gribbles Park Tuff	6,048–6,098/50	Not recognized	Not deep enough	5,470–5,840/370	2,765–2,990/225	6,020–6,295/275	6,430 to >6,581/>151	6,934–7,174/240	9,324 to >9,490/>166
Conejos Formation	3,488–7,810/4,322	5,268 to >8,023/>2,755	5,520 to > 6,831/>1,311	3,700–6,370/2,670	2,490–4,310/1,820	6,012–6,680/668	6392 to >6581/>189	6,928–7,364/436	9,324 to >9,490/>166
Formation at base Oligocene	Eocene	Not deep enough	Not deep enough	Eocene	Eocene	Precambrian	Not deep enough	Precambrian	Not deep enough
Total depth (ft)	10,350	8,023	6,831	7,125	6,072	7,011	6,581	7,474	9,490
Samples	U.S.G.S.	U.S.G.S /I.S.L.M.	No samples	Private	U.S.G.S.	Private	No samples	No samples	Private, U.S.G.S.

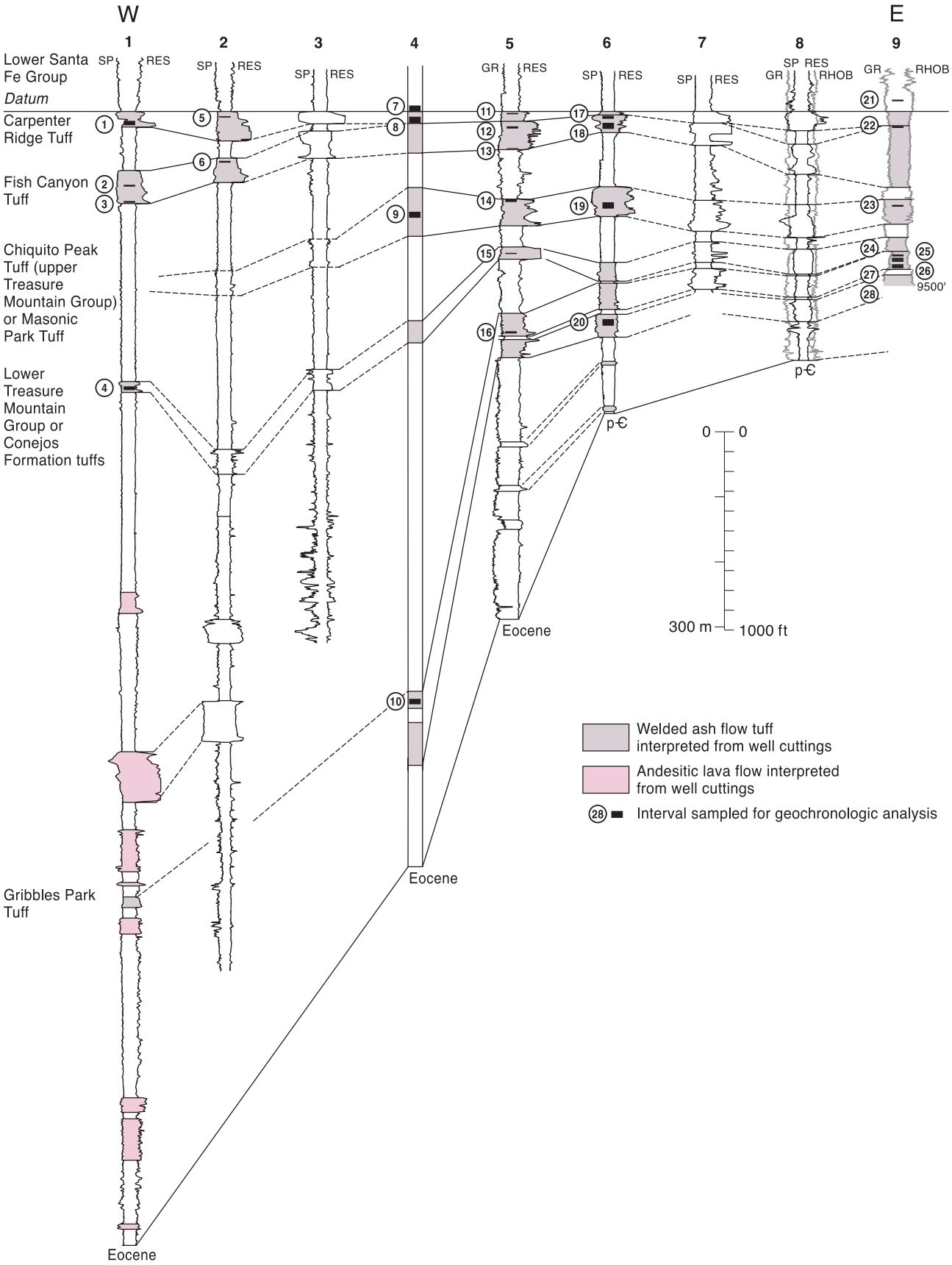

FIGURE 4—West-east statigraphic cross section from wells 1 through 9 depicted in Figure 2. Correlations are dashed where inferred. Intervals sampled for geochronologic analysis are noted by circled sample number. The stratigraphic datum is the top of Carpenter Ridge Tuff based on well-log interpretation. The horizontal scale is arbitrary and the vertical scale is noted. See Table 2 for details concerning the depths of the various stratigraphic units. **SP** = spontaneous potential log, **RES** = resistivity log, **GR** = gamma ray log, **RHOB** = bulk density log.

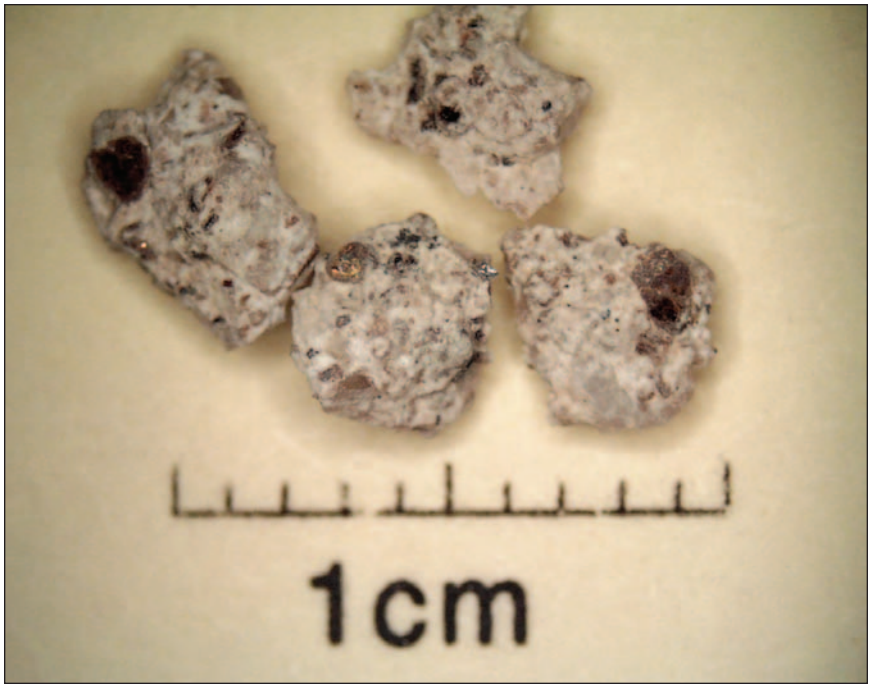

FIGURE 5—Photograph showing typical size of well cuttings from the Alamosa Basin. Sample is from the Fish Canyon Tuff in samples from the depth range of 2,440–2,450 ft (744–747 m) in well 1. Scale bar is 10 mm wide.

sequence. These logs were unavailable over the depth interval of interest in well number 9, apparently due to logging difficulties; therefore gamma ray and density logs were substituted in that well.[1]

Well cuttings representing parts of the Oligocene strata in six wells (wells 1, 2, 4, 5, 6, and 9) were examined to identify and sample probable ignimbrite units for geochronology. Samples were obtained from private collections and from the U.S. Geological Survey core facility in Denver, Colorado. No samples were available for wells 3, 7, and 8. Sample amounts available for geochronologic analysis ranged from a few cutting chips (Fig. 5) to several grams of chips. Lack of sufficient cutting chips prevented sampling of all tuffs in some wells.

Limitations of well cuttings as samples for geochronology

Figure 6 demonstrates the drilling process and factors that affect the quality and reliability of well cuttings as representative samples of a drilled interval. During drilling, fluid (mud) is pumped down the inside of drill pipe. At the bottom of the string of drill pipe, the mud exits through holes in the drill bit and returns up the annulus (outside) of the drill pipe to return to the surface. The mud is screened to remove solids generated by the drilling process and then is returned to the drill pipe by the mud pump. One of the purposes of the mud is to clean the hole of drilling solids and to carry this material to the surface for examination. In this process, millimeter-size rock chips are lifted away from the bit, preventing them from being reground. Another function of the mud is to cake (coat) the borehole wall to prevent fluid infiltration and keep the wall from eroding or disintegrating. Drilling mud varies in chemistry, viscosity, density, and, consequently, its ability to lift the cuttings and build a protective mudcake. The time it takes drilling mud to carry cuttings to the surface (termed "lag") varies within and between wells and makes it difficult to accurately determine ("depth-correct") the depth from which cuttings originate.

Additionally, flow of drilling mud up the annulus is variably turbulent due to borehole rugosity (surface roughness), telescoping borehole diameter, and washouts (localized borehole diameter excursions). Turbulence may cause cuttings to become mixed with previously drilled cuttings or with fragments derived from the borehole wall (such contaminants are typically termed "cavings" in the drilling industry). Also, the mud/cuttings separation process at the rig is typically crude, and the personnel assigned to the task are often the least experienced members of the drilling crew and may be uneducated as to the diligence required for collecting samples accurately and "on time." The sum of these problems is that when cuttings are examined after drilling (sometimes years later, as in the case of this study), evaluating which well cuttings accurately represent correctly determined depths requires a combination of careful comparison to geophysical logs, subjective elimination of probable cavings, and a fair amount of estimation of factors such as lag-time errors.

Applying high-resolution geochronologic methods to such low-resolution samples is a somewhat dubious process. We attempted to mitigate this concern by careful sample selection from the center of thick ignimbrites, as identified from cutting petrology and well-log signatures, with the assumption that the resulting ages would be representative of the sampled unit. As the results reported here show, although the effects of caving contamination are unavoidable, they can be recognized and subjectively eliminated by hand picking of cuttings and by using single-crystal dating methods.

Comparison to outcrop samples

For this project, we used geochronology rather than petrology to identify specific regional ignimbrites, but petrology aided in selection of samples for geochronologic analysis. Outcrop samples representative of established regional ignimbrites were collected, and thin sections were prepared for comparison with well cuttings. Most samples were from the San Juan Mountains, but one previously unnamed welded ignimbrite was collected from the Sangre de Cristo Range east of Fort Garland (Fig. 2). A sample of this biotite-rich ignimbrite, described by Kearney (1983) as possibly correlative to the Treasure Mountain Group (informally termed here the "tuff of Sangre de Cristo Creek"), was dated (sample 90-6; Table 3; Appendix 1). This sample locality is the only reported outcrop of ignimbrite on the east side of the northern San Luis Basin. Based on its 29.95 Ma age, the tuff of Sangre de Cristo Creek probably correlates with one of the ignimbrites in the lower Treasure Mountain Group of the San Juan volcanic field, although there are some problems with this interpretation, as discussed below.

Cutting examination methodology

The well cuttings used for this research were selected from archived collections, typically stored in bags sequentially

[1]The petroleum industry has not adopted metric standards of measurement in the United States, thus log depths and thickness noted in the figures and tables are expressed in feet. Approximate metric conversions are included in the text.

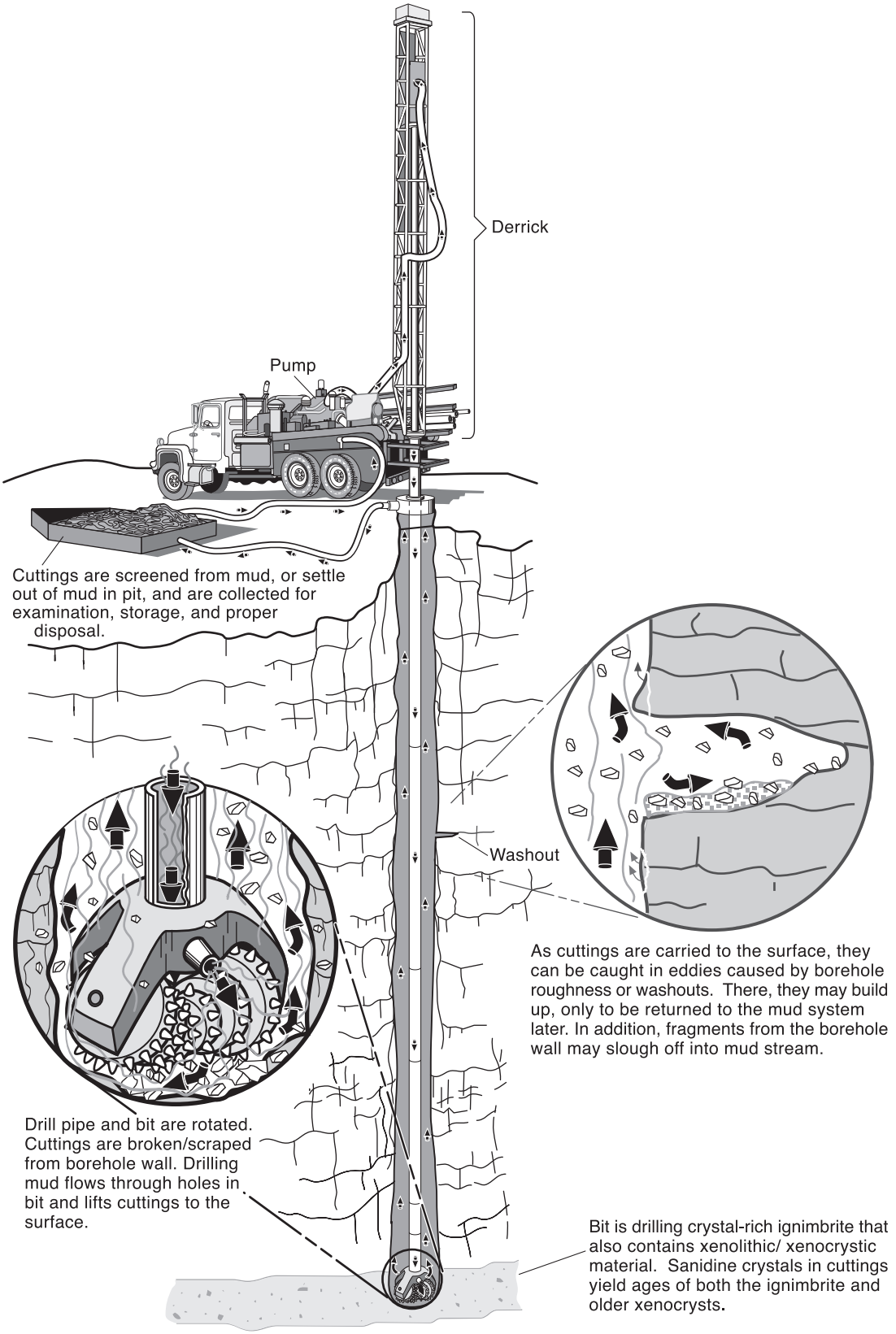

FIGURE 6—Cartoon illustrating drilling operation, circulation of drilling mud, and method of obtaining well cuttings.

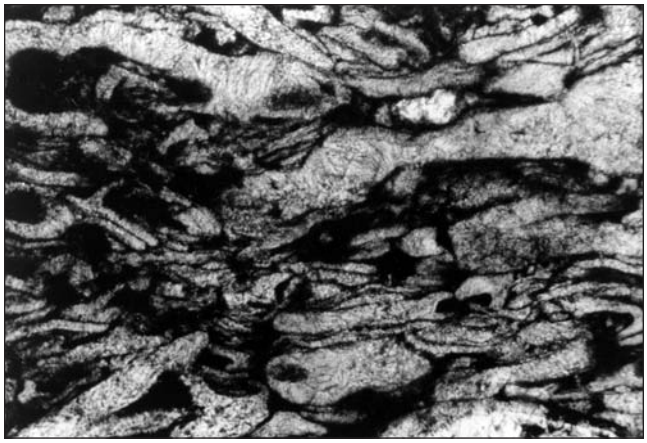

FIGURE 7—Thin section photomicrograph of welded Carpenter Ridge Tuff from approximate depth of 649 m (2,130 ft), well 1, western Alamosa Basin. Field of view is 1 mm (width).

labeled in 10 ft (3 m) intervals. Lag-time errors in the depth assignment of well cuttings were assessed by comparing the first appearance and abundance of welded-tuff cuttings with high electrical resistivity on geophysical logs. Depth corrections were applied where necessary. By examining samples sequentially from top to bottom within individual wells, many cavings were recognized and eliminated. Cuttings were examined by binocular microscope and, where sample volume allowed, thin sections were prepared to confirm lithology (Fig. 7). Recognition of ignimbrites in well cuttings was made primarily on the basis of texture, particularly evidence of eutaxitic textures characteristic of incipient to dense welding. Identifying first appearance of a new unit by petrology (e.g., color, crystal size, texture, and composition) was critical for distinguishing between ignimbrite units that were closely spaced in depth. Voluminous regional ignimbrites were initially identified on the basis of thickness, well-log character, and distinctive petrology, particularly phenocryst content.

Petrophysical characteristics of ignimbrites

Readers unfamiliar with well logs and petrophysical interpretation techniques are referred to Asquith (1982) for a basic reference on the subject. Well-log interpretation and correlation were helpful for identifying ignimbrites and other stratigraphic units within Alamosa Basin wells, particularly where well cuttings were of low quality or were not available. The ignimbrites in the Alamosa Basin that are strongly welded have distinctive corresponding geophysical signatures. The most obvious correlation is with the electrical resistivity log. Resistivity appears to mimic welding zonation, where the most resistive units correspond to tuffs that are most densely welded. In this case, resistivity typically exceeds 10 times that of the interlayered volcaniclastic units or nonwelded tuffs. The formation density log was similarly useful in well number 9 where a resistivity log was unavailable. Most of the wells predate the availability of density logs. Welded units also tend to show negative deflection of the spontaneous potential curve relative to interlayered volcaniclastic units and nonwelded tuffs. A less reliable indicator of tuffs is the gamma-ray log that was available for only three wells. Elevated gamma ray values aided in identification of some ignimbrites in well number 9.

$^{40}Ar/^{39}Ar$ geochronology

The successful use of $^{40}Ar/^{39}Ar$ geochronology of well cuttings to identify regional ignimbrites in the subsurface depends critically on several factors, including: 1) sufficient cutting fragments from known depths must be available, 2) single cuttings must be dated to required precision, and 3) the chronology of surface outcrops of regional ignimbrites must be sufficiently well established for comparison. The following paragraphs consider these three requirements.

The first requirement for geochronologic identification of subsurface ignimbrites is that cuttings fragments from ignimbrite intervals must be available in sufficient quantity and size for dating, ideally accompanied by minimal contaminants. Previous sections discussed the difficulty of determining accurate depths of origins for cuttings, and explained the origin of ubiquitous contaminant cuttings, which are typically anomalously young fragments derived from up hole (cavings). Anomalously old fragments could result from xenolithic or xenocrystic contamination, or from older clasts in sedimentary intervals. Such anomalous cutting fragments can in some cases be recognized and removed by hand picking or other methods. In practice, contaminants are not always entirely removed before dating, so mixed populations of multiple ages are expected to be common, not rare, even in carefully selected samples of well cuttings. Mixed populations of well cuttings can still yield high-precision single-cutting dates suitable for correlation purposes, *provided that data from anomalous contaminants can be recognized and weeded out by inspection, leaving a single population of age data from representative cuttings*. The subjective judgment required to make these decisions can be bolstered by attention to stratigraphic order and well-log correlations among adjacent wells.

The second requirement for geochronologic identification of subsurface ignimbrites, that available cuttings must be precisely datable, depends on the nature of the dating method employed and on the cuttings themselves. An effective analytical approach for the problem is $^{40}Ar/^{39}Ar$ laser-fusion of individual sanidine crystals. This single-crystal approach allows identification of individual age populations of crystals, and precludes misinterpretations based on mixing of multiple age populations, a problem inherent in multicrystal (bulk) analyses. The well-established single-crystal laser-fusion method (Deino and Potts 1990; Gansecki et al. 1998; McIntosh and Chamberlin 1994) can date typical individual sanidine crystals as small as 250 μm to a precision of ± 1% or better. This level of precision, in the case of the present study, is sufficient to distinguish among most potentially correlative regional ignimbrites. In this study, sanidine crystals from well cuttings exist both as loose crystals (not uncommonly abraded) and as phenocrysts within lithic fragments. Lithic fragment cuttings have the advantage of providing matrix textures for evaluation of whether the fragments represent ignimbrites or other contaminant lithologies. In practice, the largest sanidine crystals are commonly loose within the cuttings. Many lack clinging groundmass, preventing assessment of groundmass texture. It is not possible to readily assess whether these crystals were derived from ignimbrites in the drilled interval or were derived from cavings, xenoliths, or non-ignimbrite lithologies. However, in spite of their questionable heritage, loose crystals have the distinct advantage of being larger than phenocrysts within lithic cuttings, so they can be dated more precisely. As described below, both types of sanidine crystals were dated in this study.

For the majority of samples, only sanidine crystals were analyzed. Single-crystal dating of biotite was employed for a few sanidine-poor or sanidine-free samples. A multicrystal bulk biotite separate was analyzed from the one outcrop sample in this study, because the potential for biotite contamination was deemed low and the bulk step-heating approach allowed increased precision relative to single-crystal analyses.

TABLE 3—Summary of $^{40}Ar/^{39}Ar$ results from Alamosa Basin well cuttings. **L#** is laboratory number, **Irrad** is irradiation batch, **Sample type** is material from which crystals were separated (lithic = eutaxic cutting fragments only, bulk = loose crystals plus lithic cuttings), **n** is number of analyses used in mean, **nt** is total number of analyses, **K/Ca** and **Age** are mean values calculated for population of crystals interpreted as representing subsurface ignimbrite

Well	Sample	Field number	L#	Irrad	Sample type	Mineral	Age analysis	n	nt	K/Ca	Age	±2σ	Correlative regional ignimbrite
1	1	Tenn 2120-40	50713	NM-115	lithic	sanidine	laser fusion	12	14	44.1	27.37	0.09	Carpenter Ridge
1	2	Tenn 2440-50	50711	NM-115	lithic	sanidine	laser fusion	14	14	60.1	27.79	0.09	Fish Canyon
1	3	Tenn 2530-40	50712	NM-115	lithic	sanidine	laser fusion	0	8	low precision data			?
1	4	Tenn 3460-80	50716	NM-115	lithic	biotite	laser fusion	14	14	19.0	30.17	0.23	lower Treasure Mountain?
2	5	Tuck 3675	50723	NM-115	lithic	sanidine	laser fusion	10	10	40.7	27.44	0.09	Carpenter Ridge
2	6	Tuck 3900-05	50724	NM-115	lithic	sanidine	laser fusion	12	12	55.0	27.92	0.10	Fish Canyon
4	7	ES 2500-30	5078	NM-33	bulk	sanidine	laser fusion	6	10	11.9	23.21	0.30	?
4	8	ES 2560-90	5077	NM-33	bulk	sanidine	laser fusion	2	2	91.2	27.22	0.15	Carpenter Ridge
4	9	ES 3040-70	5076	NM-33	bulk	sanidine	laser fusion	4	9	13.1	28.91	0.21	Chiquito Peak?
4	10	ES 5500-30	50720	NM-115	lithic	sanidine	laser fusion	7	8	60.4	32.92	0.11	Gribbles Park
5	11	Amer 1760-70	51248	NM-123	bulk	sanidine	laser fusion	16	19	58.5	27.70	0.16	?
5	11	Amer 1760-70	50714	NM-115	lithic	biotite	laser fusion	15	15	14.6	32.68	0.40	?
5	12	Amer 1820-30	51247	NM-123	bulk	sanidine	laser fusion	9	10	69.6	27.79	0.09	?
5	12	Amer 1820-30	50719	NM-115	lithic	biotite	laser fusion	14	14	9.7	32.32	0.19	?
5	13	Amer 1930	51265	NM-123	bulk	sanidine	laser fusion	2	2	72.2	27.76	0.11	?
5	13	Amer 1930	50715	NM-115	lithic	biotite	laser fusion	11	14	18.5	32.58	0.32	?
5	14	Amer 2180-2200	51251	NM-123	bulk	sanidine	laser fusion	10	12	49.8	27.79	0.19	?
5	14	Amer 2180-2200	50722	NM-115	lithic	biotite	laser fusion	12	15	16.4	32.17	0.40	?
5	15	Amer 2460-70	51266	NM-123	bulk	sanidine	laser fusion	6	7	36.3	28.03	0.15	?
5	16	Amer 2860-70	51250	NM-123	bulk	sanidine	laser fusion	3	4	63.0	27.76	0.28	?
5	16	Amer 2860-70	50721	NM-115	lithic	biotite	laser fusion	14	14	11.7	32.24	0.30	?
6	17	Res 5180-90	51286	NM-123	bulk	sanidine	laser fusion	1	4	44.5	25.13	0.09	?
6	18	Res 5210-40	5079	NM-33	bulk	sanidine	laser fusion	5	8	15.0	27.88	0.14	?
6	19	Res 5610-40	51267	NM-123	bulk	sanidine	laser fusion	12	13	58.6	27.40	0.58	?
6	20	Res 6200-30	51285	NM-123	bulk	sanidine	laser fusion	5	5	60.2	27.93	0.39	?
9	21	Map 8560-70	51249	NM-123	bulk	sanidine	laser fusion	0	2	multimodal data			?
9	21	Map 8560-70	50718	NM-115	lithic	sanidine	laser fusion	0	5	all plagioclase			?
9	22	Map 8690-8700	50717	NM-115	lithic	sanidine	laser fusion	10	10	60.9	28.00	0.15	Fish Canyon
9	23	Map 9090-9100	5075	NM-33	bulk	sanidine	laser fusion	0	4	all xenocrysts			?
9	24	Map 9304-50	6202	NM-45	bulk	sanidine	laser fusion	10	12	57.8	32.90	0.12	Gribbles Park
9	25	Map 9360-70	6199	NM-45	bulk	sanidine	laser fusion	11	14	54.7	32.86	0.12	Gribbles Park
9	26	Map 9370-80	6201	NM-45	bulk	sanidine	laser fusion	11	15	54.6	32.84	0.14	Gribbles Park
9	27	Map 9390-9400	6200	NM-45	bulk	sanidine	laser fusion	13	15	82.0	33.03	0.19	Gribbles Park
9	28	Map 9400-9410	6203	NM-45	bulk	sanidine	laser fusion	13	15	58.2	32.77	0.13	Gribbles Park
tuff of Sangre de Cristo Creek													
outcrop	29	Brister 90-6	50725	NM-115	outcrop	biotite	furnace step heat	12	12	24.5	29.95	0.12	lower Treasure Mountain?

Methods:

Sample preparation: crushing, LST heavy liquid, Franz, HF, hand-picking.

Irradiation: four separate in vacuo 7–14 hr irradiations (NM-33, NM-45, NM-115, NM-123), D-3 position, Nuclear Science Center, College Station, TX.

Neutron flux monitor: sample FC-1 of interlaboratory standard Fish Canyon Tuff sanidine with an assigned age of 27.84 Ma (Deino and Potts 1990), equivalent to Mmhb-1 at 520.4 Ma (Samson and Alexander 1987); samples and monitors irradiated in alternating holes in machined Al discs.

Laboratory: New Mexico Geochronology Research Laboratory, New Mexico Institute of Mining and Technology, Socorro, NM.

Instrumentation: Mass Analyzer Products 215-50 mass spectrometer on line with automated, all-metal extraction system.

Heating: sanidine and biotite from cuttings—single-crystal laser-fusion, 10W continuous CO_2 laser; bulk biotite from outcrop sample—3.7 mg aliquot in resistance furnace.

Reactive gas cleanup: SAES GP-50 getters operated at 20°C and ~450°C; SCLF—1–2 min., RFIH—9 min.

Error calculation: all errors reported at ±2 σ, means ages calculated using inverse variance weighting of Samson and Alexander (1987),

Decay constant and isotopic abundances: Steiger and Jaeger (1977).

Complete data set in Appendix.

Analytical parameters:

Electron multiplier sensitivity = 1 to 3 x 10^{-17} moles/pA; typical system blanks were 470, 3 , 0.6 , 3, 3.0 x 10^{-18} moles (laser) and 1,800, 38, 1.5, 5, 8(furnace) at masses 40, 39, 38, 37, 36 respectively; . J-factors determined to a precision of ± 0.2% using SCLF of 4–6 crystals from each of 4–6 radial positions around irradiation vessel. Correction factors for interfering nuclear reactions, determined using K-glass and CaF_2, ($^{40}Ar/^{39}Ar$) K = 0.00020 ± 0.0003; ($^{36}Ar/^{37}Ar$) Ca = 0.00026 ± 0.00002; and ($^{39}Ar/^{37}Ar$) Ca = 0.00070 ± 0.00005.

The third requirement for geochronologic identification of subsurface ignimbrites is the necessity of having a well-constrained chronology for exposed regional ignimbrites that can be compared with data from subsurface ignimbrites. The stratigraphy and chronology of potentially correlative regional ignimbrites in south-central Colorado is relatively well established. Understanding of the complex geologic history of the regional volcanic fields has been enhanced by decades of field- and laboratory-based studies, which have included mapping, observations of superposition, measurements of flow direction, determination of areal distribution of units, and studies of petrology, geochemistry, and paleomagnetism (e.g., Lipman et al. 1970, 1996; Epis and Chapin 1974; Steven and Lipman 1976; Lanphere 1988). $^{40}Ar/^{39}Ar$

sanidine or biotite age determinations for 30–23 Ma San Juan volcanic field ignimbrites are summarized in Lipman (2000). A $^{40}Ar/^{39}Ar$ sanidine-based chronology and stratigraphic framework has also recently been developed for the 37–32 Ma regional ignimbrites of the adjacent Central Colorado volcanic field (McIntosh and Chapin this volume). Table 1 summarizes $^{40}Ar/^{39}Ar$ ages of selected regional ignimbrites from these two volcanic fields.

Sample preparation and analysis

Two types of samples were prepared from well cuttings drilled from ignimbrite intervals: 1) sanidine crystals separated from bulk samples containing both lithic fragments and free crystals, and 2) sanidine or biotite crystals separated from lithic fragments only (free crystals excluded). The terms "bulk" and "lithic" are used to distinguish between the sample types in Table 3, Figures 8 and 9, and Appendix 1. In both sample types, obvious contaminant cuttings were removed by hand picking. Most bulk samples included large, matrix-free sanidine crystals, similar in size to rock fragments in the cuttings (typically 1–3 mm in diameter). These larger crystals may have been liberated from the rock groundmass by the drill bit and be representative of the ignimbrite drilled, or they may originate from xenolithic or xenocrystic material (older rock fragments entrained in the ignimbrite) or other non-ignimbrite lithologies. Alternatively, groundmass-free crystals may come from up-hole contaminants (cavings) derived from the borehole wall during drilling. In the lithic sample type, lithology and texture of the matrix aids interpretation of the origin of individual fragments, allowing removal of many apparent contaminating lithic components. Unfortunately, phenocrysts contained within individual lithic cutting fragments tend to be relatively small, in some cases too small to yield precise results.

Rock fragments from both bulk and lithic samples were lightly crushed to free crystals from enclosing matrix, then sanidine crystals were separated using a combination of standard magnetic, density liquid, and hand-picking methods. Biotite was separated from some rock-fragment samples that lacked sanidine. Sanidine and/or biotite separates from a total of 29 well-cutting samples and biotite from the one outcrop sample (sample number 90-6) were deemed suitable for $^{40}Ar/^{39}Ar$ analysis. Fish Canyon Tuff sanidine with an assumed age of 27.84 Ma (Deino and Potts 1990) was included as a monitor mineral during irradiation and analysis. Single crystals of sanidine, biotite, and monitor sanidine were analyzed by CO_2 laser fusion at the New Mexico Geochronology Research Laboratory. A bulk aliquot of biotite separate from the single outcrop sample (90-6 in Appendix 13-Brister-01) was analyzed using resistance-furnace step-heating. Details of separation and analytical methods are included in the footnote to Table 3, and the complete analytical data are presented in Appendix 1.

Analytical results

Single-crystal laser-fusion $^{40}Ar/^{39}Ar$ analyses yielded generally precise, accurate age determinations for most of the sanidine crystals analyzed in this study. The precision ($\pm 2\sigma$) for most of the analyses is between $\pm$ 0.3% and $\pm$ 1%. Some of the smaller crystals yielded less precise results; sanidine analyses with precision worse than $\pm$ 2% were disregarded. $^{40}Ar/^{39}Ar$ dates obtained from biotite are somewhat less precise than the sanidine results. The precision of single-crystal biotite analyses typically ranged from $\pm$ 0.6% to $\pm$ 3%; analyses with precision worse than $\pm$ 4% were discarded. The one outcrop sample analyzed by bulk step-heating of biotite yielded a flat age spectrum and a weighted mean age with a precision of $\pm$ 0.4%.

Precise single-crystal results were obtained from all but two of the 28 cutting samples dated in this study. As a first-pass filter of the data, single-crystal data were discarded if they were insufficiently precise (criteria described above), if their K/Ca ratios indicated a plagioclase composition ($K/Ca < 0.5$), or if they yielded pre-Cenozoic ages indicating xenocrystic or detrital contamination. Results from two samples were discarded following this first-pass filtering. One (sample 3, Appendix 1) had small crystals that yielded imprecise results, and the other (sample 21, Appendix 1) contained only one crystal that was not pre-Cenozoic. Of the 26 samples that yielded precise results, 16 samples from four wells (wells 1, 2, 4, and 9; Fig. 8) yielded data that are readily interpretable and support correlations with regional ignimbrites. Interpretation of results from ten samples from the remaining two wells (wells 5 and 6) is problematic, as discussed below.

Of the 16 samples with readily interpretable results, nine (samples 2, 4, 5, 6, 8, 10, 22, 24, and 28; Table 3; Fig. 4) yielded simple, single-mode age populations. Data from five other samples (samples 1, 9, 25, 26, and 27; Fig. 8) are slightly multimodal. The majority of dated crystals from each of these samples form a single dominant mode, accompanied by a small minority of crystals with aberrant ages interpreted as being due to caving or xenocrystic contamination. The two remaining samples (samples 7 and 21; Fig. 8) both from the base of the Santa Fe Group, yield strongly multimodal ages. This multimodality probably reflects detrital origin with crystals derived from various ignimbrites eroded from the volcanic field. The ages of populations of crystals from wells 1, 2, 4, and 9, with single-mode or slightly multimodal age distributions, closely match the ages of regional ignimbrites in the adjacent San Juan and Central Colorado volcanic fields. Proposed correlations are shown in Figures 4 and 8 and are further discussed in later sections; these ages and proposed correlations agree well with stratigraphic order and with correlations among wells based on cutting petrology and well-log characteristics.

Data from wells 5 and 6 (Fig. 9) are problematic and cannot readily be used to identify regional ignimbrites. Single-crystal data from samples from well 5 are paradoxically bimodal in both lithology and age. All five samples from a variety of depths contain loose sanidine crystals and biotite-rich eutaxitic cuttings but lack sanidine-bearing lithic cuttings. Virtually all of the analyzed biotites yielded apparent single-crystal ages near 32 Ma, whereas the sanidines yielded ages ranging from 28 to 23 Ma. The consistent coexistence of 32-Ma biotite-rich lithic fragments with much younger (possibly caved) loose sanidine crystals throughout much of the volcanic interval in this well is difficult to explain, as is the lack of a stratigraphic progression of ages among either the sanidine or the biotite. Four samples of cuttings from well 6 lacked sanidine- or biotite-rich lithic cuttings. Loose sanidine crystals from these four samples, like those from well 5, lack any apparent systematic relationship between drilling depth and age. We are uncertain why cutting samples from wells 5 and 6 produced confusing and unsystematic results. The average size of lithic cuttings from these wells was unusually fine, which may have effectively increased the relative amount of contaminants in the cutting samples. Alternatively, the samples from these two wells may not have been collected in a systematic manner during drilling so that the depths assigned to the dated cutting samples may be inaccurate. In any case, age data from samples from wells 5 and 6 were disregarded and were not applied to ignimbrite correlations.

Alamosa Basin stratigraphy interpreted from geochronologic results

One of the goals for this project was to develop a methodol-

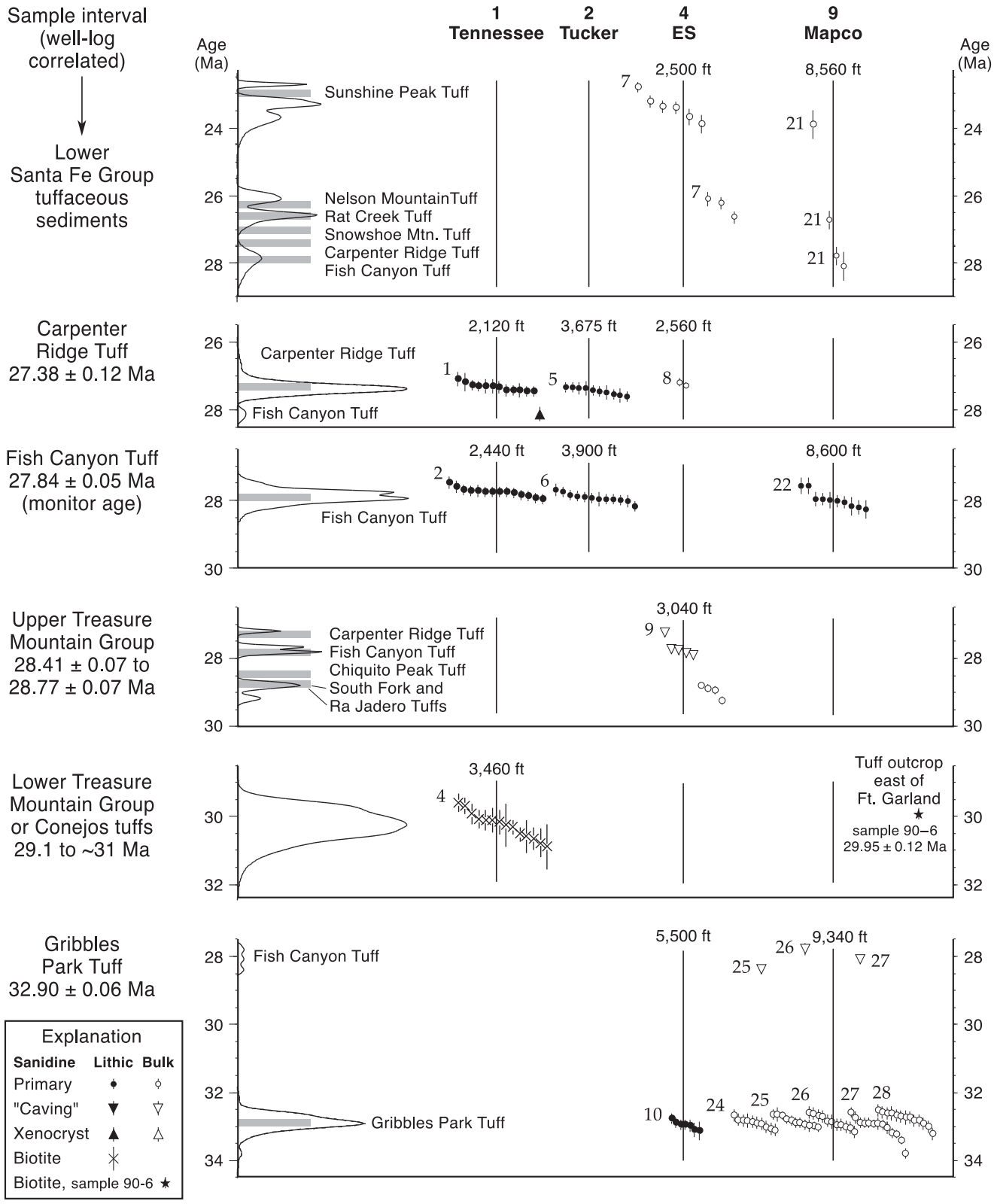

FIGURE 8—Compilation of single-crystal $^{40}Ar/^{39}Ar$ results from wells 1, 2, 4, and 9. Each point depicts a single-crystal date with ± 1σ error bars. Symbols for sample type, mineralogy, and interpretation of each data point are identified in the explanation. Groups of points represent data from individual samples, numbered as in Table 3. Four-digit number above each group of data points is sample depth in feet. Curves at left are relative probability distributions (Deino and Potts 1992) for the cumulative single-crystal data from each sampling interval. Gray bands along these curves and text along the left margin provide names and ages of probable correlative regional ignimbrites.

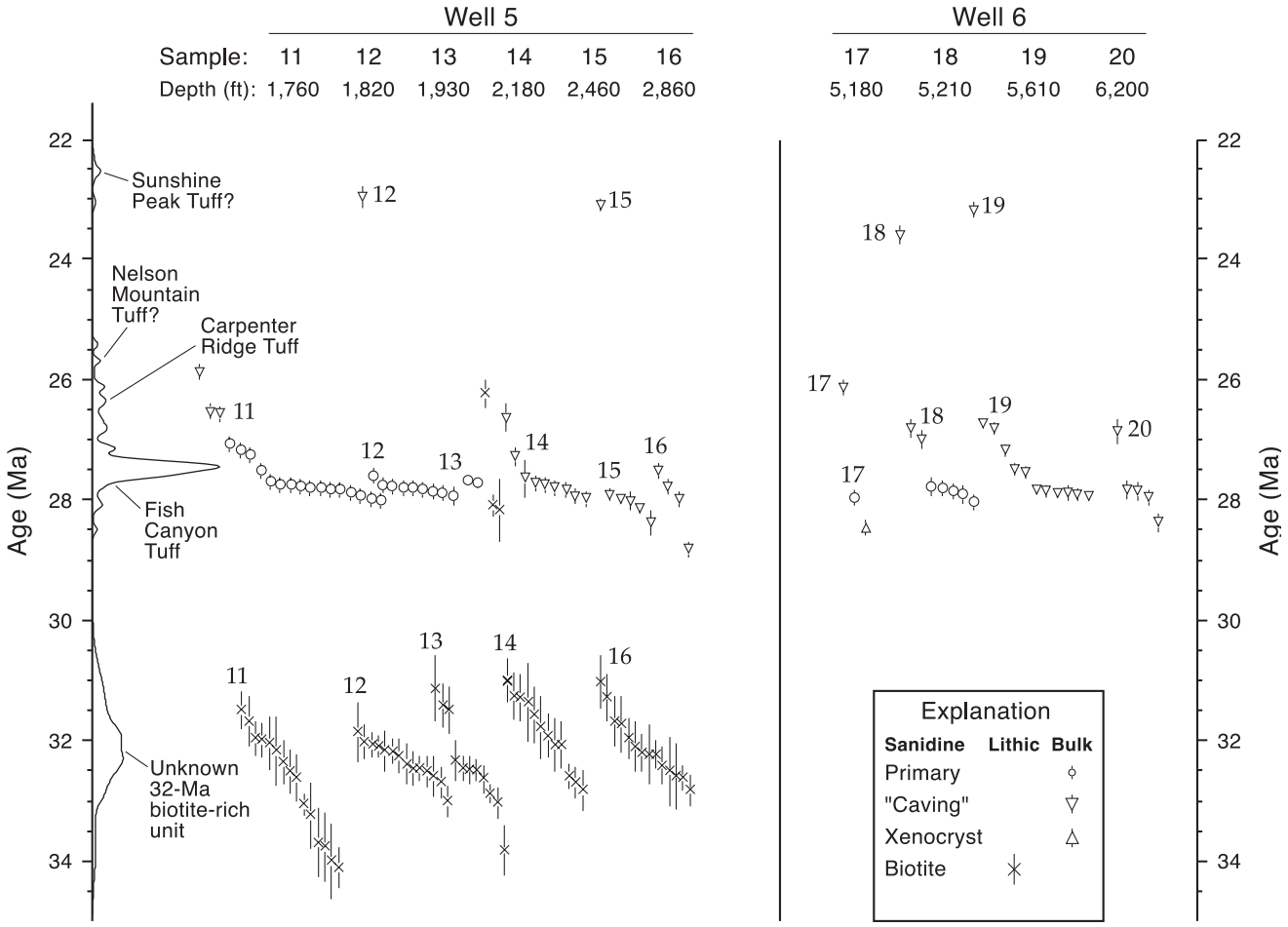

FIGURE 9—Compilation of problematic single-crystal $^{40}Ar/^{39}Ar$ results from wells 5 and 6. As in Figure 8, each point depicts a single-crystal date with ± 1σ error bars and groups of points represent data from individual samples, numbered as in Table 3. Symbols for sample type and mineralogy are identified in the explanation. In contrast to Figure 8, samples from different depths are arrayed horizontally across the diagram, with sample depths shown at the top of the figure. Curves at left show relative probability distributions that are cumulative for all of the data from wells 5 and 6. It is difficult to explain the consistent presence of both 32-Ma biotite-rich lithic fragments and much younger loose sanidine crystal throughout the thickness of well 5. Also puzzling is the lack, in both wells 5 and 6, of a stratigraphic progression of ages among either the sanidine or the biotite. Possible explanations for these problematic data are discussed in the text.

ogy for selecting samples from well cuttings that would yield reliable analytical results. Another was to confirm and refine the volcanic stratigraphy of an area that is buried beneath thousands of feet of post-volcanic basin fill by correlation with dated volcanic units in adjacent exposed areas. In this paper, we demonstrate that specific tuffs can indeed be correlated among adjacent wells, across the basin, and to outcrops. One advantage in applying geochronology to borehole cuttings in the Alamosa Basin is that the entire subsurface stratigraphic section at any one location can be quantified in terms of age, stratigraphic position, and thickness of units. This advantage would be particularly useful for other undissected depositional basins where outcrops are limited or entirely unavailable.

The Oligocene volcanic and volcaniclastic sequence in the Alamosa Basin includes a lower part derived from both the San Juan and Central Colorado volcanic fields and an upper part derived entirely from the San Juan volcanic field. The lower part consists primarily of intermediate composition volcaniclastic deposits and subordinate andesitic lava flows, in part erupted from the nearby Summer Coon stratovolcano (denoted on Fig. 2), and assigned to the Conejos Formation (Lipman 1968) of the San Juan volcanic field. Interlayered with the Conejos Formation is the Gribbles Park Tuff, a regional rhyolitic ignimbrite erupted from the Bonanza caldera (Varga and Smith 1984) of the Central Colorado volcanic field (McIntosh and Chapin 2004 this volume). The upper part of the Oligocene sequence contains several voluminous ignimbrites from San Juan volcanic field calderas, west of the Alamosa Basin (Fig. 2; Table 1). The densely welded Carpenter Ridge Tuff (Olson et al. 1968; Lipman 2000), selected as the stratigraphic reference datum in Figure 4, is a distinctive marker near the top of the sequence that is easily recognized as an electrically-resistive unit in geophysical logs and as a strong-amplitude peak in seismic records (Brister and Gries 1994). Other prominent welded tuffs are the Fish Canyon Tuff (Olson et al. 1968; Lipman 2000), upper Treasure Mountain Group sanidine-bearing tuffs (Lipman et al. 1970, 1996), and lower Treasure Mountain Group sanidine-free, biotite-rich tuffs (Lipman and Steven 1970; Lipman 1975; Lipman et al. 1996). Interlayered with the San Juan volcanic field welded tuffs are volcaniclastic deposits including fluvial sandstone, conglomerate and shale, eolian sandstone, and nonwelded and/or reworked tuffs.

Figure 4 summarizes interpretations of the subsurface

volcanic stratigraphy and the distribution of specific regional ignimbrites within the Alamosa Basin. In general, the ignimbrites thicken and thin from well to well, independent of the cumulative thickness of the entire volcanic sequence. There is no evidence from our data for discrete, temporally persistent paleovalleys, in contrast to the persistent paleovalleys in the Central Colorado volcanic field to the north described by McIntosh and Chapin (2004 this volume). Instead, the ignimbrites appear to have blanketed the region, implying generally subdued aggradational paleotopography. The ignimbrites probably originally extended eastward at least as far as the present Sangre de Cristo Range, but they have since been eroded at the surface. Each dated formation is discussed in more detail separately below, from oldest to youngest.

Conejos Formation and Gribbles Park Tuff

Well cuttings and geophysical logs indicate that intermediate-composition volcaniclastic sediments and lavas dominate the lower parts of the volcanic interval in each of the nine studied wells in the Alamosa Basin. This interval is interpreted to be equivalent to the Conejos Formation as defined by Lipman (1989). Volcaniclastic rocks of the Conejos Formation include volcanic breccias, matrix-supported boulder mudflow deposits, massive boulder-cobble fluvial conglomerates, and a variety of fluvial to lacustrine sandstone and mudstone deposits. Minor tuffs from vents in the San Juan volcanic field have also been documented (e.g., Tuff of Rock Creek of Dungan et al. 1989). Within the San Juan volcanic field, the Conejos Formation is overlain by the Treasure Mountain Group (approximately 29.5 Ma; Lipman 2000).

Because the Conejos andesitic interval lacks sanidine or biotite, it was not directly dated in the course of this study, although the 30.17 ± 0.23 Ma age of the overlying biotite-rich tuff provides a minimum age constraint and the interlayered 32.9 Ma Gribbles Park Tuff provides an additional age constraint. The Conejos Formation appears to thin markedly eastward from a thickness of 1,317 m (4,322 ft) in well 1, to 133 m (436 ft) in well 8, which equates to eastward thinning at a rate of approximately 28 m per km (57 ft per mi). Similarly, andesitic lava flows within the Conejos Formation thin dramatically eastward (Fig. 4). This is consistent with the Conejos Formation in the Alamosa Basin being derived from the Summer Coon stratovolcano and others to the west (Lipman 1968) rather than from local vents within the basin. It is also possible that some of this interval in the Alamosa Basin is derived from sources farther north in the Central Colorado volcanic field (McIntosh and Chapin 2004 this volume). The eastward thinning of the Conejos Formation section suggests that it was thin or absent as far east as the present Sangre de Cristo Range. This reinforces the conclusion of Brister and Gries (1994) that Conejos-type clasts in the Miocene and younger rift-valley fill of the Alamosa Basin were derived from erosion of the west flank of the rift valley, rather than from the east flank. The thickness distribution of the Conejos clearly suggests that the western Monte Vista graben of the Alamosa Basin was subsiding during Conejos deposition. In the Monte Vista graben, the Conejos Formation overlies Eocene red beds that accumulated in the precursor Monte Vista pull-apart basin attributed to late Laramide wrench faulting (Brister and Chapin 1994). The coincidence of thickening of the two formations in this area suggests that the wrench-related Laramide basin was reactivated during regional Oligocene tectonic extension.

Interlayered within the lower third of the Conejos Formation interval in the Alamosa Basin is a rhyolitic ignimbrite interpreted as the Gribbles Park Tuff, the youngest regional ignimbrite in the Central Colorado volcanic field, erupted from the Bonanza caldera at 32.9 Ma. Heretofore the Gribbles Park Tuff was not known to exist in the San Luis Basin south of the Bonanza caldera at the northern end of the basin. Sanidine crystals from this interval in wells 4 and 9 yielded ages of 32.9 Ma. Gribbles Park Tuff or related dacitic units are probably also present in wells 1, 5, and 6, although no datable sanidines were obtained from these wells. Estimating the thickness of the Gribbles Park Tuff is problematic due to inconclusive geophysical log control, but it ranges from a minimum of approximately 15 m (50 ft) in well 1 to a maximum of approximately 113 m (370 ft) in well 4. Several wells drilled in the San Juan Mountains west of the Summer Coon volcano have penetrated tuffs in the lower Conejos Formation (B. S. Brister, unpublished research); one of these tuffs could potentially correlate to the Gribbles Park Tuff.

Lower Treasure Mountain Group

Lower Treasure Mountain Group ignimbrites are recognizable in the subsurface of the Alamosa Basin as a series of stacked sanidine-poor, biotite-rich, thin tuffs that generally lack well-log evidence for strong welding. Average thickness of the composite unit in wells 1 through 9 is 27 m (89 ft). In outcrop in the San Juan volcanic field, the lower Treasure Mountain Group includes three biotite-rich, sanidine-free large-volume ignimbrites erupted from the Platoro caldera: Ojito Creek Tuff (29.1 ± 0.3 Ma), La Jara Canyon Tuff (29.3 ± 0.3 Ma), and Black Mountain Tuff (29.4 ± 0.4 Ma; Balsley 1994; Lipman et al. 1996). The only data obtained from this interval in the subsurface of the Alamosa Basin is the 30.17 ± 0.23 Ma biotite age derived from well 1 (Figs. 4, 8). Although this age determination is somewhat older than published age determinations from the lower Treasure Mountain Group (Balsley 1994; Lipman et al. 1996), it agrees closely with the 29.95 ± 0.12 Ma age determined from the lithogically similar tuff of Sangre de Cristo Creek (outcrop sample 90-6, Table 3), exposed in the Sangre de Cristo Mountains east of well 9. The similarity of lithology and $^{40}Ar/^{39}Ar$ ages suggests that the dated biotite-rich tuff in well 1 correlates with the tuff of Sangre de Cristo Creek, representing a San Juan ignimbrite that was extensive enough to cross the entire width of the Alamosa Basin. The regional correlation of this ignimbrite is somewhat uncertain. The sanidine-free, biotite-rich lithology, together with the fact that the ignimbrite directly overlies Conejos-like andesitic lavas, strongly suggests a correlation with one of the ignimbrites in the lower Treasure Mountain Group. In contrast, the discrepancy between our 30 Ma age determinations and the published 29.1–29.4 Ma ages for the lower Treasure Mountain Group suggests that this ignimbrite might actually be a tuff within the 29.4–33.1 Ma Conejos Formation (Colucci et al. 1991; Lipman et al. 1996). However, ignimbrites in the generally andesitic Conejos Formation typically lack phenocrystic biotite (Colucci et al. 1991). Resolution of this correlation problem will require additional work.

Upper Treasure Mountain Group

One or more sanidine-bearing upper Treasure Mountain Group ignimbrites are interpreted to be present in eastern Alamosa Basin wells 4 through 9, although they are thin in well 3 and absent in wells 1 and 2. Dated upper Treasure Mountain Group sanidine-bearing ignimbrites in the San Juan volcanic field (Table 1) include Chiquito Peak Tuff (28.4 Ma), South Fork Tuff (28.8 Ma), and Ra Jadero Tuff (28.8 Ma), all erupted from the Summitville/Platoro caldera complex (Lipman et al. 1996; Lipman 2000). Masonic Park Tuff (28.6 Ma), erupted from the Mount Hope caldera of the San

Juan volcanic field, has a similar age but lacks sanidine (Lipman et al. 1996; Lipman 2000). The upper Treasure Mountain Group interval in the subsurface of the Alamosa Basin has an average thickness in wells 3 through 9 of 48 m (157 ft). The absence, or near-absence, of this unit in wells 1, 2, and 3 may be due to local blocking of the path of the outflow sheet by the preexisting Summer Coon volcano. Only one sample (sample 9, well 4) from the entire upper Treasure Mountain Group interval was successfully dated. It yielded a few sanidine crystals with a 28.5 ± 0.2 Ma age, suggesting correlation with the 28.4 Ma Chiquito Peak Tuff.

Fish Canyon Tuff

The 27.8 Ma Fish Canyon Tuff was positively identified in wells 1, 2, and 9, and is almost certainly present in other wells. The Fish Canyon Tuff, erupted from the La Garita caldera, is the most voluminous regional ignimbrite of San Juan volcanic field and one of the largest known ignimbrites in the world, with an estimated volume in excess of 5,000 km^3 (Lipman 2000). Geophysical logs and well-cutting lithology indicate that the Fish Canyon Tuff is strongly welded across the entire width of the Alamosa Basin. The contact of the Fish Canyon Tuff with the overlying Carpenter Ridge Tuff is indistinct in some wells. Average thickness of this ignimbrite in the subsurface of the Alamosa Basin is approximately 48 m (156 feet). It generally thins gradually eastward; although it appears to be thickest in the easternmost well (well 9). This interpretation is probably, in part, an artifact of lack of definitive resistivity log data in that well. Fish Canyon Tuff from Alamosa Basin wells contains abundant large (1–3 mm) sanidine crystals. Free crystals from this unit, apparently dislodged from the borehole wall during drilling, are the greatest contributor of caving contaminant crystals in well-cutting samples from underlying units (Figs. 8, 9).

Carpenter Ridge Tuff

The uppermost welded tuff identifiable from well logs and cuttings is the 27.3 Ma Carpenter Ridge Tuff, which was erupted from the Bachelor caldera and is the second largest outflow sheet in the San Juan volcanic field (volume > 1,000 km^3; Lipman 2000). Virtually all sanidine crystals from this interval in wells 1, 2, and 4 yielded ages near 27.3 Ma, in close agreement with ages determined from outcrops of Carpenter Ridge Tuff (Lipman 2000; McIntosh and Chapin 2004 this volume). Carpenter Ridge Tuff can be identified in the remaining wells on the basis of being the shallowest welded tuff. There is some uncertainty about the lower contact of the Carpenter Ridge Tuff in wells 6, 7, and 9 where it apparently rests directly on the Fish Canyon Tuff. Thickness of the Carpenter Ridge Tuff in Alamosa Basin wells ranges from 6 to 50 m (from 20 to 164 ft), averaging 22 m (72 ft), with no apparent directional trends in thickness.

Santa Fe Group

Petrologic and petrophysical characteristics suggest that the Carpenter Ridge Tuff is overlain in several wells by tuffaceous sandstone. Geochronology reveals that samples collected near the base of the Santa Fe Group contain mixed-provenance sanidine crystals derived from San Juan volcanic field ignimbrites. Sanidine crystals from this interval in wells 4 and 9 correspond to the Sunshine Peak Tuff (22.9 Ma, Lake City caldera, beyond the western edge of Fig. 2), Nelson Mountain Tuff (26.4 Ma, San Luis caldera), and Fish Canyon Tuff (27.8 Ma, La Garita caldera). Above these basal samples, the Santa Fe Group contains increasingly higher concentrations of lithic fragments derived from the Conejos Formation and Precambrian rocks.

Conclusions

Confirmation of regional ignimbrites within basin

The analytical results of this geochronologic study confirm the observations of Brister and Gries (1994) concerning the presence and significance of ignimbrites within the Alamosa Basin. High-precision $^{40}Ar/^{39}Ar$ dating now allows conclusive correlation with established regional ignimbrites and mapping of their extent within the limitations of the well control. Regional outflow sheets appear to have blanketed subdued aggradational topography across the area. In addition, the well control demonstrates that the Oligocene volcanic sequence rests directly on Precambrian basement in the eastern half of the basin. This has negative implications for petroleum exploration seeking Cretaceous targets in the basin. Given that the top of the welded Carpenter Ridge Tuff is an excellent seismic reflector (Brister and Gries 1994), seismic methods can be used to map this marker as an approximate base of the Santa Fe Group. The Santa Fe Group is an important aquifer in the basin; having the capability to accurately determine its thickness and extent could aid in our understanding of regional water resources

An important new discovery is that the Gribbles Park Tuff is now known to have a larger extent than previously determined, definitely existing within the basin south of the Bonanza caldera, where it appears to have blanketed a broad area. This contrasts with its distribution in the Central Colorado volcanic field where it is found mainly within paleovalleys. Its apparent widespread distribution raises the possibility that it may also be found interlayered with the lower Conejos Formation in the San Juan Mountains.

Early-stage tectonic extension and basin subsidence

The Oligocene volcanic and volcaniclastic sequence described in this paper clearly preserves a record of an early- or pre-rift period of tectonic extension. Subsidence and associated accumulation of bimodal volcanic rocks in the Alamosa Basin began before 32.9 Ma, the age of the Gribbles Park Tuff, and perhaps as early as 35 Ma, the probable maximum age assigned to the Conejos Formation in the San Juan volcanic field (Lipman et al. 1970). This closely matches observations made elsewhere in the Rio Grande rift region (e.g., Cather 1989, Mack et al. 1994), where an early extensional event preceded the formation of axial rift basins at about 26 Ma (Chapin and Cather 1994). A fundamental change in the morphology of the Alamosa Basin occurred after Carpenter Ridge Tuff emplacement (post-27.3 Ma). The beginning of rift-related east tilting is marked by an unconformity developed upon the Carpenter Ridge Tuff (Lipman and Mehnert 1975). The unconformity is exposed on the southwestern flank of the Alamosa Basin where the Hinsdale Basalt lies upon the unconformity (Lipman 1976). Farther south, the Hinsdale Basalt has a maximum approximate age of 25–27 Ma (Lipman and Mehnert 1975; Thompson et al. 1986; Thompson and Machette 1989; Chapin and Cather 1994). The Hinsdale Basalt is absent in the wells studied here; therefore in wells 4 and 9, where the unconformity was roughly bracketed by geochronology, the unconformity is younger than 27.3 Ma (age of the Carpenter Ridge Tuff) but older than lower Santa Fe Group sediments that contain 22.9-Ma sanidine and are thus younger than 22.9 Ma.

Potential applications in other basins

The potential for application of $^{40}Ar/^{39}Ar$ geochronology to well cuttings in other basins and volcanic fields is very good, provided that volcanic units containing suitable minerals for dating are present. Successful identification of regional volcanic units using well cuttings is most likely to succeed where regional stratigraphy has already been well

established, where single-crystal dating methods are applied to subjectively selected well cutting samples, and where results are interpreted in conjunction with independent forms of data such as geophysical well logs.

Acknowledgments

The authors acknowledge Charles E. "Chuck" Chapin, who has devoted much of his career to the study of the tectonic development and Tertiary stratigraphy of the Southern Rocky Mountain region. Chuck has instilled a strong interest in these topics in his many students, the authors included. Robbie Gries and Dick Burroughs assisted in locating private collections of well cuttings and provided useful related well information. The U.S. Geological Survey Core Research Center allowed access to key well cuttings analyzed for this study. Mineral separations and geochronologic analyses were performed by Richard Esser, Lisa Peters, and other staff of the New Mexico Geochronology Research Lab at New Mexico Institute of Mining and Technology. Thanks to reviewers Chuck Chapin, Steve Cather, and Ren Thompson.

References

Asquith, G. B., 1982, Basic well log analysis for geologists: American Association of Petroleum Geologists, 216 pp.

Balsley, S. D., 1994, A combined stratigraphic, chronologic, and petrologic study of an Oligocene post-collapse pyroclastic sequence, southeastern San Juan Mountains, Colorado—the middle tuff member of the Treasure Mountain Tuff: Unpublished Ph.D. dissertation, Southern Methodist University, 214 pp.

Bove, D. J., Hon, K., Budding, K. E., Slack, J. F., Snee, L. W., Yeoman, R. A., 2000, Geochronology and geology of late Oligocene through Miocene volcanism and mineralization in the western San Juan Mountains, Colorado: U.S. Geological Survey, Open-file Report OF 99-0347, 33 pp.

Brister, B. S., and Chapin, C. E., 1994, Sedimentation and tectonics of the Laramide San Juan sag, Southwestern Colorado: The Mountain Geologist, v. 31, no. 1, pp. 2–18.

Brister, B. S., and Gries, R. R., 1994, Tertiary stratigraphy and tectonic development of the Alamosa Basin (northern San Luis Basin), Rio Grande rift, south-central Colorado; *in* Keller, G. R., and Cather, S. M. (eds.), Basins of the Rio Grande rift—structure, stratigraphy, and tectonic setting: Geological Society of America, Special Paper 291, pp. 39–58.

Burroughs, R. L., 1981, A summary of the geology of the San Luis Basin, Colorado and New Mexico, with emphasis on the geothermal potential for the Monte Vista graben: Colorado Geological Survey, Special Publication 17, 30 pp.

Cather, S. M., 1989, Post-Laramide tectonic and volcanic transition in west-central New Mexico; *in* Anderson, O. J., Lucas, S. G., Love, D. W., and Cather, S. M. (eds.), Southeastern Colorado Plateau: New Mexico Geological Society, Guidebook 40, pp. 91–97.

Chapin, C. E., 1971, The Rio Grande rift; Part I, Modifications and additions; *in* James, H. L. (ed.), San Luis Basin: New Mexico Geological Society, Guidebook 22, pp. 191–201.

Chapin, C. E., and Cather, S. M., 1994, Tectonic setting of the axial basins of the northern and central Rio Grande rift; *in* Keller, G. R., and Cather, S. M. (eds.), Basins of the Rio Grande rift—structure, stratigraphy, and tectonic setting: Geological Society of America, Special Paper 291, pp. 5–23.

Colucci, M. T., Dungan, M. A., Ferguson, K. M., Lipman, P. W., and Moorbath, S., 1991, Precaldera lavas of the southeast San Juan volcanic field—parent magmas and crustal interactions: Journal of Geophysical Research, v. 96, no. B8, pp. 13,413–13,434.

Cordell, L., 1978, Regional geophysical setting of the Rio Grande rift: Geological Society of America, Bulletin, v. 89, no. 7, pp. 1073–1090.

Deino, A. L., and Potts, R., 1990, Single-crystal of $^{40}Ar/^{39}Ar$ dating of the Olorgesailie Formation, southern Kenya rift: Journal of Geophysical Research, v. 95, no. B6, pp. 8453–8470.

Dungan, M. A., Thompson, R. A., Stormer, J. S., O'Neill, J. M., 1989, Rio Grande rift volcanism—northeastern Jemez zone, New Mexico; *in* Chapin, C. E., and Zidek, J. (eds.), Field excursions to volcanic terranes in the western United States, Volume I—Southern Rocky Mountain region: New Mexico Bureau of Mines and Mineral Resources, Memoir 46, pp. 435–486.

Epis, R. C., and Chapin, C. E., 1974, Stratigraphic nomenclature of the Thirtynine Mile volcanic field, central Colorado: U.S. Geological Survey, Bulletin 1395-C, 23 pp.

Epis, R. C., and Chapin, C. E., 1975, Geomorphic and tectonic implications of the post-Laramide, late Eocene erosion surface in the Southern Rocky Mountains; *in* Curtis, B. F. (ed.), Cenozoic history of the Southern Rocky Mountains: Geological Society of America, Memoir 144, pp. 45–74.

Gansecki, C. A., Mahood, G. A., and McWilliams, M., 1998, New ages for the climactic eruptions at Yellowstone; single-crystal $^{40}Ar/^{39}Ar$ dating identifies contamination: Geology, v. 26, no. 4, pp. 343–346.

Gries, R. R., 1985, Seismic lines in the San Luis Valley, south-central Colorado; *in* Gries, R. R., and Dyer, R. C. (eds.), Seismic exploration of the Rocky Mountain region: Rocky Mountain Association of Geologists and Denver Geophysical Society, pp. 267–274.

Kearney, B. C., 1983, Volcanic stratigraphy and structure of the La Veta Pass area, northern Sangre de Cristo Mountains, south-central Colorado: Unpublished M.S. thesis, Southern Methodist University, 67 pp.

Keller, G. R., Cordell, L., Davis, G. H., Peeples, W. J., and White, G., 1984, A geophysical study of the San Luis Basin; *in* Baldridge, W. S., Dickerson, P. W.., Riecker, R. E., and Zidek, J. (eds.), Rio Grande rift—northern New Mexico: New Mexico Geological Society, Guidebook 35, pp. 51–58.

Kluth, C. F., and Schaftenaar, C. H., 1994, Depth and geometry of the northern Rio Grande rift in the San Luis Basin, south-central Colorado; *in* Keller, G. R.,and Cather, S. M. (eds.), Basins of the Rio Grande rift—structure, stratigraphy, and tectonic setting: Geological Society of America, Special Paper 291, pp. 27–37.

Lanphere, M. A., 1988, High-resolution of $^{40}Ar/^{39}Ar$ chronology of Oligocene volcanic rocks, San Juan Mountains, Colorado: Geochimica et Cosmochimica Acta, v. 52, pp. 1425–1434.

Lipman, P. W., 1968, Geology of Summer Coon volcanic center, eastern San Juan Mountains, Colorado; *in* Epis, R. C. (ed.), Cenozoic volcanism in the Southern Rocky Mountains: Colorado School of Mines, Quarterly, v. 63, no. 3, pp. 211–236.

Lipman, P. W., 1975, Evolution of the Platoro caldera complex and related volcanic rocks, southeastern San Juan Mountains, Colorado: U.S. Geological Survey, Professional Paper 852, 128 pp.

Lipman, P. W., 1976, Geologic map of the Del Norte area, eastern San Juan Mountains, Colorado: U.S. Geological Survey, Miscellaneous Investigations Map I-952, scale 1:48,000.

Lipman, P. W., 1989, Oligocene–Miocene San Juan volcanic field, Colorado, Introduction; *in* Chapin, C. E., and Zidek, J. (eds.), Field excursions to volcanic terranes in the western United States, Volume I—Southern Rocky Mountain region: New Mexico Bureau of Mines and Mineral Resources, Memoir 46, pp. 303–305.

Lipman, P. W., 2000, Central San Juan caldera cluster—regional volcanic framework; *in* Bethke, P. M., and Hay, R. L. (eds.), Ancient Lake Creede—its volcano-tectonic setting, history of sedimentation, and relation to mineralization in the Creede mining district: Geological Society of America, Special Paper 346, pp. 9–69.

Lipman, P. W., and Mehnert, H. H., 1975, Late Cenozoic basaltic volcanism and development of the Rio Grande depression in the Southern Rocky Mountains; *in* Curtis, B. F. (ed.), Cenozoic history of the Southern Rocky Mountains: Geological Society of America, Memoir 144, pp. 119–154.

Lipman, P. W., and Steven, T. A., 1970, Reconnaissance geology and economic significance of the Platoro caldera, southeastern San Juan Mountains, Colorado: U.S. Geological Survey, Professional Paper 700-C, pp. C19–C29.

Lipman, P. W., Steven, T. A., and Mehnert, H. H., 1970, Volcanic history of the San Juan Mountains, Colorado, as indicated by potassium-argon dating: Geological Society of America, Bulletin, v. 81, no. 8, pp. 2329–2352.

Lipman, P. W., Dungan, M. A., Brown, L. L., and Deino, A., 1996, Recurrent eruption and subsidence at the Platoro caldera complex, southeastern San Juan volcanic field, Colorado—new tales from old tuffs: Geological Society of America, Bulletin, v. 108, no. 8, pp. 1039–1055.

Mack, G. H., Nightengale, A. L., Seager, W. R., and Clemons, R. E., 1994, The Oligocene Goodsight–Cedar Hills half graben near Las

Cruces and its implications to the evolution of the Mogollon–Datil volcanic field and the southern Rio Grande rift; *in* Chamberlin, R. M., Kues, B. S., Cather, S. M., Barker, J. M., and McIntosh, W. C. (eds.), Mogollon Slope, west-central New Mexico and east-central Arizona: New Mexico Geological Society, Guidebook 45, pp. 135–142.

McIntosh, W. C., and Chamberlin, R. M., 1994, $^{40}Ar/^{39}Ar$ geochronology of middle to late Cenozoic ignimbrites, mafic lavas, and volcaniclastic rocks in the Quemado region, New Mexico; *in* Chamberlin, R. M., Kues, B. S., Cather, S. M., Barker, J. M., and McIntosh, W. C. (eds.), Mogollon slope: New Mexico Geological Society, Guidebook 45, pp. 165–185.

McIntosh, W. C., and Chapin, C. E., 2004, Geochronology of the Central Colorado volcanic field, Colorado; *in* Cather, S. M., McIntosh, W. C., and Kelley, S. A. (eds.), Tectonics, geochronology, and volcanism in the Southern Rocky Mountains and Rio Grande rift: New Mexico Bureau of Geology, Bulletin 160, pp. 205–238.

Olson, J. C., Hedlund, D. C., and Hansen, W. R., 1968, Tertiary volcanic stratigraphy in the Powderhorn–Black Canyon region, Gunnison and Montrose Counties, Colorado: U.S. Geological Survey, Bulletin 1251-C, 29 pp.

Phetteplace, D. R., and Kunze, J. F., 1983, Geothermal exploration well for the City of Alamosa, Colorado, Final Report: U.S. Department of Energy, Contract Number DE-FC07-81ID12259, 124 pp.

Samson, S. D., and Alexander, E. C., Jr., 1987, Calibration of the interlaboratory $^{40}Ar/^{39}Ar$ dating standard, Mmhb-1: Chemical Geology, v. 66, no. 1-2, pp. 27–34.

Steiger, R. H., and Jäger, E., 1977, Subcommission on geochronology—convention on the use of decay constants in geo- and cosmochronology: Earth and Planetary Science Letters, v. 36, pp. 359–362.

Steven, T. A., and Lipman, P. W., 1976, Calderas of the San Juan volcanic field, southwestern Colorado: U.S. Geological Survey, Professional Paper 958, 35 pp.

Thompson, R. A., Dungan, M. A., Lipman, P. W., 1986, Multiple differentiation processes in early-rift calc-alkaline volcanics, northern Rio Grande rift, New Mexico: Journal of Geophysical Research, v. B 91, no. 6, pp. 6046–6058.

Thompson, R. A., and Machette, M. N., 1989, Geologic map of the San Luis Hills area, Conejos and Costilla Counties, Colorado: U.S. Geological Survey, Miscellaneous Investigations Series Map I-1906, scale 1:50,000.

Tweto, O., 1979, Geologic map of Colorado: U.S. Geological Survey, scale 1:500,000.

Varga, R. J., and Smith, B. M., 1984, Evolution of the early Oligocene Bonanza caldera, northeast San Juan volcanic field, Colorado: Journal of Geophysical Research, v. 89, no. B10, pp. 8679–8694.

Watkins, T. A., 1996, Geology of the northeastern San Luis Basin, Saguache County, Colorado; *in* McGowan, I. R., Cain, D., and Smith, K. (eds.), Hydrogeology of the San Luis Valley and environmental issues downstream from the Summitville mine: Geological Society of America, Annual Meeting Field Guide, 7 p. (unpaginated).